UCRL-PROC-223922

LAWRENCE
LIVERMORE
NATIONAL
LABORATORY

# Ultrafast Coherent Diffraction Imaging with X-ray Free-Electron Lasers

H. N. Chapman, S. Bajt, A. Barty, W.H. Benner, M.J. Bogan, M. Frank, S.P. Hau-Riege, R.A. London, S. Marchesini, E. Spiller, A. Szoke, B.W. Woods, S. Boutet, K.O. Hodgson, J. Hajdu, M. Bergh, F. Burmeister, C. Caleman, G. Huldt, F.R.N.C. Maia, M. M. Seibert, D. van der Spoel

August 23, 2006

FEL 2006
Berllin, Germany
August 28, 2006 through September 1, 2006

**Disclaimer**

This document was prepared as an account of work sponsored by an agency of the United States Government. Neither the United States Government nor the University of California nor any of their employees, makes any warranty, express or implied, or assumes any legal liability or responsibility for the accuracy, completeness, or usefulness of any information, apparatus, product, or process disclosed, or represents that its use would not infringe privately owned rights. Reference herein to any specific commercial product, process, or service by trade name, trademark, manufacturer, or otherwise, does not necessarily constitute or imply its endorsement, recommendation, or favoring by the United States Government or the University of California. The views and opinions of authors expressed herein do not necessarily state or reflect those of the United States Government or the University of California, and shall not be used for advertising or product endorsement purposes.

# ULTRAFAST COHERENT DIFFRACTION IMAGING WITH X-RAY FREE-ELECTRON LASERS*

H. N. Chapman[#], S. Bajt, A. Barty, W.H. Benner, M.J. Bogan, M. Frank, S.P. Hau-Riege, R.A. London, S. Marchesini, E. Spiller, A. Szőke, B.W. Woods, LLNL, Livermore, CA 94550, U.S.A.

S. Boutet, K.O. Hodgson, SSRL, SLAC, Menlo Park, CA 94305, U.S.A.

J. Hajdu[†], Magnus Bergh, Florian Burmeister, Carl Caleman, Gösta Huldt, Filipe R.N.C. Maia, M. Marvin Seibert, David van der Spoel, U. Uppsala, S-75124 Uppsala, Sweden.

*Abstract*

The ultrafast pulses from X-ray free-electron lasers will enable imaging of non-periodic objects at near-atomic resolution [1, Neutze]. These objects could include single molecules, protein complexes, or virus particles. The specimen would be completely destroyed by the pulse in a Coulomb explosion, but that destruction will only happen after the pulse. The scattering from the sample will give structural information about the undamaged object. There are many technical challenges that must be addressed before carrying out such experiments at an XFEL, which we are doing so with experiments at FLASH, the soft-X-ray FEL at DESY.

## SINGLE PARTICLE IMAGING

The success of crystallography lies in its ability to overcome radiation damage, by spreading the X-ray dose over many (> $10^9$) identical copies of the molecule and taking advantage of the strong signal that arises from the coherent superposition of X-rays scattered from these elements (i.e. Bragg spots). However, by performing measurements with ultrashort pulses, we can apply crystallographic techniques to non-repetitive structures (including cells, viruses, and single macromolecules). The radiation dose required for such "diffraction imaging" will be orders of magnitude above the steady-state damage threshold of about 200–4000 photons/Å$^2$ (depending on sample size and wavelength) [2 Sayre and Chapman, 1995]. Even so, the high-angle (high-resolution) scattering from a single molecule will be extremely weak since, unlike diffraction from a crystal, there will be no coherent addition of scattering from many identical unit cells. We expect that the proposed XFELs will provide enough photons per pulse to give a measurable atomic-resolution signal.

Atomic-resolution imaging of biological objects with X-rays will necessarily be "lensless"; a diffraction pattern is recorded and a computer reconstruction algorithm performs the image formation step, replacing the role of a lens. Although the phase (wavefront) of the diffraction pattern is not recorded, it is possible to reconstruct the complex-valued image of a finite object from the far-field diffracted intensity. For single molecules and other non-periodic objects, the diffracted intensity is not confined to Bragg spots as it is for crystals. This allows an "oversampling" of the diffraction pattern, and the collection of information not accessible in a crystallographic experiment [3 Sayre, 1952; 4 Miao, 1999]. The "shrinkwrap" algorithm [5 Marchesini, 2003] is a particularly robust and practical method of using this information and performing 2D and 3D image reconstructions [6 Chapman, 2006].

A full 3D reconstruction can be achieved from diffraction patterns taken from many different orientations of the structure. With XFEL pulses a complete data set will require identical copies of the object exposed to the beam one by one, which may be injected into the vacuum

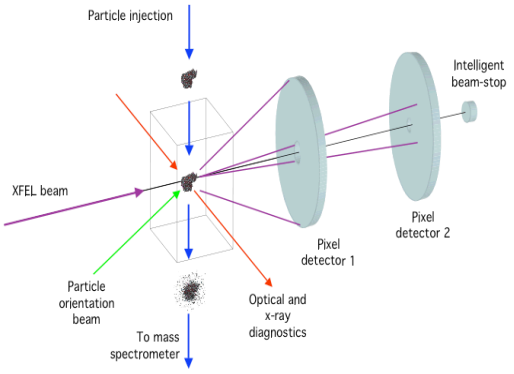


Figure 1: Schematic diagram of a single-particle diffraction imaging experiment at an XFEL.

*Work supported by U.S. Department of Energy (DOE) under Contract W-7405-Eng-48 to the University of California, Lawrence Livermore National Laboratory; the National Science Foundation Center for Biophotonics, University of California, Davis, under Cooperative Agreement PHY 0120999; The National Center for Electron Microscopy and the Advanced Light Source, Lawrence Berkeley Lab, under DOE Contract DE-AC02-05CH11231; Natural Sciences and Engineering Research Council of Canada; the U.S. Department of Energy Office of Science to the Stanford Linear Accelerator Center; the European Union (TUIXS); The Swedish Research Council; The Swedish Foundation for International Cooperation in Research and Higher Education; and The Swedish Foundation for Strategic Research.
[#]henry.chapman@llnl.gov
[†]janos.hajdu@xray.bmc.uu.se

environment of the experiment and pass through the beam path at a random orientation. With reproducible samples it will become possible to sort diffraction patterns to find those of similar orientation that can then be averaged. The averaging step will be important in order to improve the signal to noise ratio (SNR) and hence improve resolution, and the critical step in the analysis becomes finding the minimum dose that is required not to image a particle, but to infer its orientation. Hence any method that can be employed to fix a particle's orientation, such as laser alignment [7 Spence, 2004; 8 Starodub, 2005] will have a big impact on the success of the technique.

A concept of the single-particle diffraction experiment is shown in Fig. 1. Some of the challenges we face to develop this technique include: understanding the interaction of the specimen and the FEL pulse to determine how short a pulse is required to overcome radiation damage; methods to focus X-ray FEL pulses to below 0.1 micron focal spots to achieve high intensity; development of high-dynamic range, low noise, and fast area detectors; methods of delivering purified samples into the beam without containers or substrates; handling the large data stream from the detectors and performing the classification and averaging of the diffraction data; and developing robust 3D imaging techniques.

## RESOLUTION LIMITS

### *Radiation Damage*

Radiation damage significantly limits the resolution of conventional imaging experiments. Damage is caused by energy deposited into the sample by the probes used for imaging (photons, electrons, neutrons, etc.). Cooling can slow down sample deterioration, but it cannot eliminate damage-induced sample movement *during* conventional measurements [9 Henderson, 1990; 10 1995; 11 Nave 1995; 12 Howells]. Ultra short x-ray pulses from X-ray free-electron lasers offer the possibility to extend the conventional damage limits, and will allow the imaging of non-crystalline biological (and other) materials. For proteins, simulations based on molecular dynamics (MD) [1 Neutze et al., 2000; 13 Jurek et al., 2004a, 14 2004b], hydrodynamic [15 Hau-Riege et al., 2004], and on plasma models [16 Bergh *et al.*, 2004] indicate that if very short (100 fs or less) and very intense x-ray pulses are available ($\geq 10^6$ photons/Å$^2$ on the sample), then a single scattering pattern could be recorded from a single protein molecule in the gas phase before radiation damage manifests itself and ultimately destroys the sample (Figure 2).

The hydrodynamic model can be computed fast on a computer, as compared with MD models. However, the MD models are potentially more accurate since they treat the microscopic atom-atom and atom-electron interactions in greater detail. The general approach at our Laboratories is to use continuum dynamics for simulations of the soft x-ray experiments at FLASH and to quickly explore new concepts for molecular imaging at XFELs, while developing an advanced MDMC model for more accurate simulations of the x-ray-molecule interaction for XFELs.

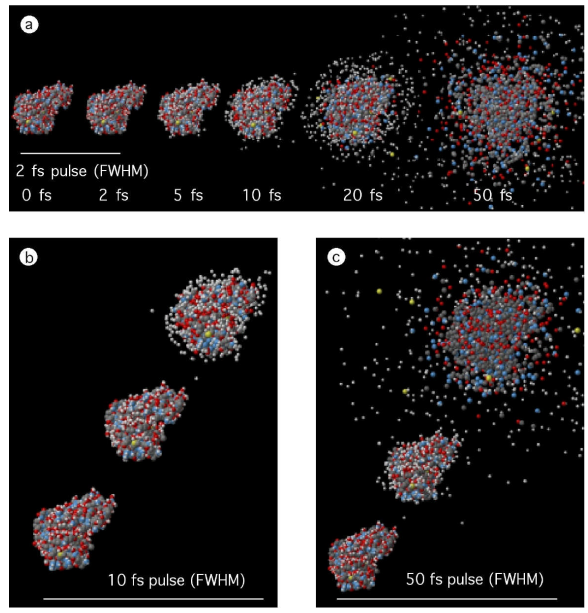


Figure 2: MD simulation of radiation-induced Coulomb explosion of a small protein (lysozyme). White balls: H, Gray: C, Blue: N, Red: O, Yellow: S. Integrated X-ray intensity: $3x10^{12}$ (12 keV) photons/100 nm diameter spot (corresponding to 3.8 x $10^8$ photons/nm$^2$, or 3.8 x $10^6$ photons/Å$^2$ on the sample) in all cases. (a) Protein exposed to a 2 fs FWHM X-ray pulse, and disintegration followed in time. The atomic positions in the first two structures (before and after the pulse) are practically identical at this pulse length due to an inertial delay in the explosion. (b) Lysozyme exposed to the same number of photons as in (a) but the pulse FWHM is now 10 fs. The images show the structure at the beginning, in the middle and near the end of the X-ray pulse. (c) Behaviour of the protein during a 50 fs FWHM X-ray pulse. It is also apparent from the figure that during the Coulomb explosion, hydrogen ions and highly ionised sulphurs are the first to escape the immediate vicinity of the protein (at 12 keV, the photoelectric cross section for sulphur is about fifty times larger than that for carbon). Based on Neutze at al. [1].

The basic assumption of the HD model is that the sample can be described by a liquid-like continuum of matter rather than considering individual atoms. This gives a simplified description of the average effects of x-ray material interaction and atomic motion, which then permits calculations even on very big samples. The model further assumes that the particle is spherically symmetric, reducing the mathematical model to one dimension plus time. The model assumes that the motion of the atoms within the molecule is solely in the radial direction. The electrons and the atoms are treated as separate, structureless, fluids that interact through the Coulomb force and ionization processes. The short-range electron-electron interactions are treated as a hydrodynamic pressure, and the long-range electron-electron and electron-ion Coulomb interactions are determined from

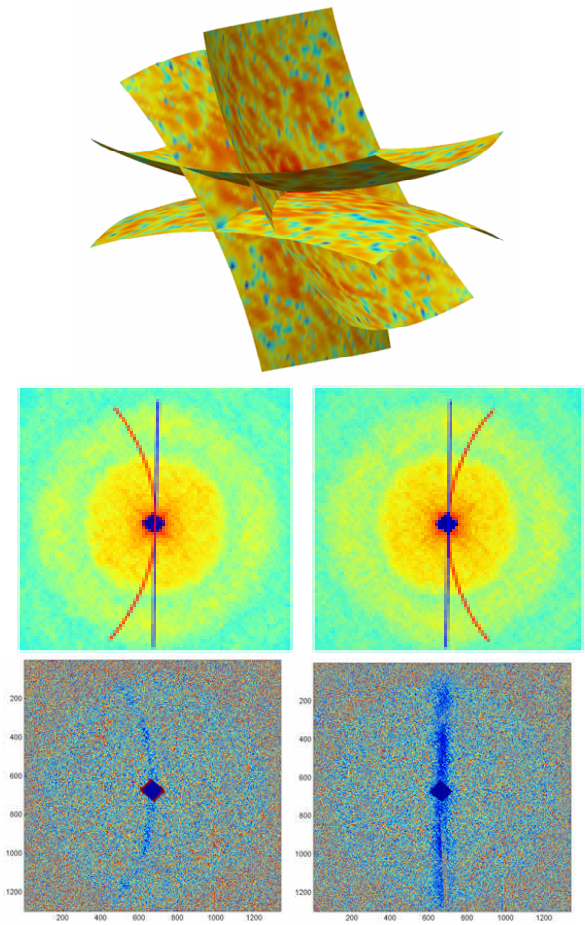


Figure 3: Intersection of two Ewald spheres with their centrosymmetric opposites. Centrosymmetry gives an extra intersect as there are *two* common arcs of intersection in *each* diffraction pattern (middle). The patterns in the middle show the expected arcs of intersections in two diffraction patterns from the experimental pyramid X-ray diffraction data set from Figure 10. Patterns at the bottom show these very lines of intersections when the experimentally obtained patterns are subtracted from each other pair wise (Huldt et al., in preparation).

the continuous net charge of the electrons and ions. In this model, all forces act radially. The model further assumes that the trapped electrons are thermalised among themselves, and that they are inertia free, so that they quickly relax to a force-free spatial equilibrium. Finally, the x-ray matter interaction, atomic ionization processes, and energy of the trapped electrons are described by time-dependent rate equations. The model shows that at later phases in an exposure, trapped electrons quickly relax in energy and position to form a cloud around the positive ions, leaving a neutral core and a positively charged outer shell (similar to Debye shielding). This layer is ejected first from the particle, and the Coulomb explosion proceeds from the outside in. A rarefaction wave propagates in from the surface at the sound speed, and hence the centre of the particle undergoes destruction later. In the inner core, there is hardly any ion motion but the high electron temperature leads to ionization and blurring of the electron density.

This behaviour has led to the proposal of a tamper as a sacrificial layer that will delay the onset of damage on the structure of interest [17 London, 2006]. The tamper may be a small water or helium drop that surrounds the molecule, and which has a total mass comparable to that of the molecule. Modern electrospray techniques can precisely control the amount of solvent left around the molecule and can be used to select an optimum layer thickness.

## *Sample reproducibility and orientation*

Each particle (macromolecule) is exposed to the beam only once, and disintegrates at the end of this process. The diffraction pattern so recorded encodes a two-dimensional projection image of the sample (and this may provide sufficient information for some applications). Three-dimensional imaging requires more than one view from the sample. In addition, the signal-to-noise ratio of raw diffraction images will probably be insufficient for a high-resolution reconstruction, and it will be necessary to obtain a redundant data set so that averaging can enhance the signal. One could extend the depth of view from a single exposure by various holographic techniques based on external or internal reference beams, but a full three-dimensional reconstruction will most likely require *reproducible samples* exposed to the beam one-by one, and in different orientations. A "reproducible sample" (e.g. purified proteins) may contain heterogeneities, different subgroups of sample, and distinct conformers of the molecule. How reproducible is a "reproducible sample" and how well can we distinguish between similar and dissimilar structures will affect resolution through a B-factor-like component.

Conventional "single molecule" electron cryo-microscopy [18 Frank, 1996; 19 van Heel et a. 2000] faces similar challenges as those described here. The basic requirement for reconstruction and/or signal averaging from many diffraction images is the ability to tell whether two noisy diffraction patterns represent the same view of the sample or two different views [20 Huldt et al. 2003]. Huldt *et al.* [20 Huldt et al. 2003] have shown that a signal of less than one photon per pixel would be sufficient to correlate diffraction images of identical particles presenting the same view, assuming photon noise only. Correlation-based methods to average and orient large numbers of noisy, randomly oriented real-space images have been successfully developed in the electron microscopy community [18 Frank, 1996; 19 van Heel et al., 2000]. Diffraction patterns are first classified into classes of like-orientation so that they can be averaged to increase the signal relative to noise [20 Huldt et al., 2003]. The average signal per diffraction pattern at the highest resolution, required for

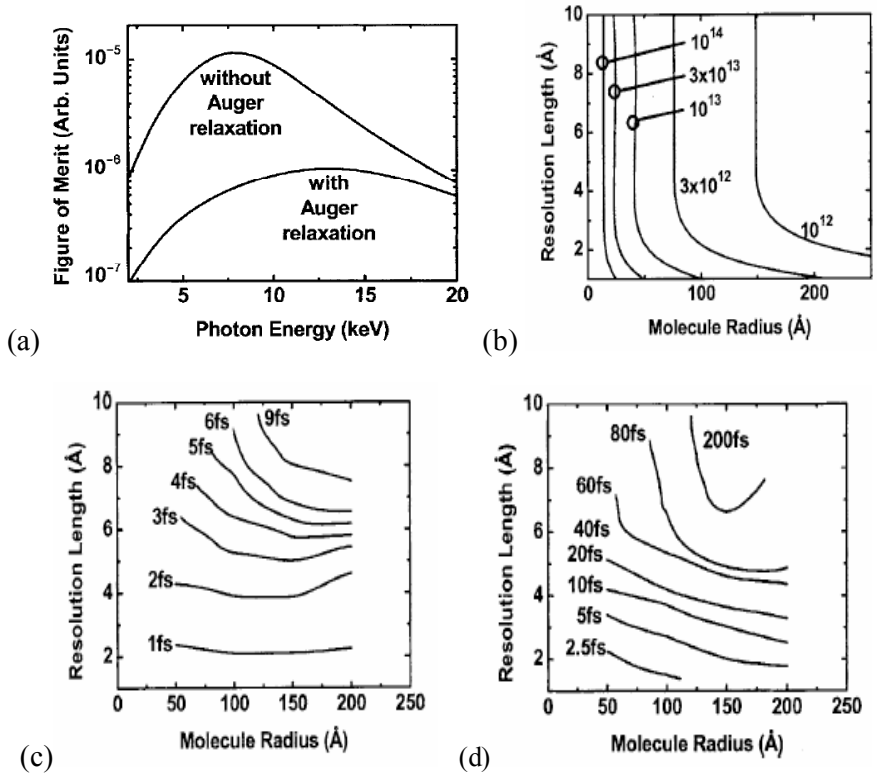


Figure 4: Resolution vs. radius for different X-ray fluences. (a) FOM for imaging conditions as a function of photon energy. (b) X-ray fluence requirements to classify two-dimensional diffraction patterns of biological molecules according to their orientation with 90% certainty. The curves are labeled with the X-ray fluence in units of photons in a 100 nm spot. (c) Plot of achievable resolution vs. molecule size for various pulse durations as limited by damage and classification. Atomic resolution imaging is achievable with pulse durations less than 5 fs and fluences greater than $10^{12}$ photons per 0.1 micron spot size. (d) Pulse duration requirements are significantly relaxed for samples that give 10 times larger scattering signal (e.g. viruses or nanocrystals). (Hau-Riege *et al.,* in preparation)

classification, is found to be much less than one photon per pixel, and an incident fluence of $10^8$ ph/nm$^2$ is sufficient to achieve atomic resolution for particles greater than 15 nm radius [20 Huldt et al., 2003].

Averaged diffraction patterns must be oriented with respect to each other in 3D Fourier space, which may be achieved by the method of common lines, a technique widely used in electron microscopy, where the micrographs represent planar sections through the center of the molecular transform. X-ray diffraction patterns are recorded on the Ewald sphere and so two patterns of different orientations will intersect along an arc in reciprocal space that passes through the zero spatial frequency. If the signal is strong enough for the line of intersection to be found in two averaged images, it will then be possible to establish the relative orientation of these patterns. We note that due to the curvature of the sections (especially at X-ray wavelengths), the common arc will provide a three-dimensional fix rather than a hinge-axis. Moreover, since the electron density of the object is real, its molecular transform exhibits centrosymmetry. This symmetry ensures that we obtain two independent repeats of the common lines in the two images. This feature provides redundancy for determining sample orientation, and is unique to diffraction patterns (Figure 3).

## *Resolution for reproducible particles*

A combination of results from the hydrodynamic continuum model [15 Hau-Riege et al., 2004] with the diffraction pattern classification model of Huldt et al. [20] allows one to map out the landscape of imaging resolution, molecule size and pulse requirements [21 Hau-Riege et al, 2005]. The results are shown in Figure 4, which show that it will be possible to image single molecules at very high resolutions with very short pulse durations (atomic resolution with pulses less than about 5-10 fs).

First, the optimal photon energy for diffraction imaging was estimated by maximizing a figure of merit (FOM), defined as the ratio of signal minus noise to the radiation damage. As shown in Figure 4a, for pulses shorter than the Auger decay time (~10 fs for C), the optimum photon energy is 8 keV, and for longer pulses it is 13 keV,

although the peak FOM is much smaller. Figure 4b shows the required x-ray fluence versus image resolution length and particle radius, required to achieve a large enough diffraction signal to classify the patterns. Figure 4c shows the pulse length requirements for x-ray imaging biological molecules with 12 keV photons, assuming no pre-orientation of the molecules. When the fluence requirements are relaxed by orienting molecules with laser fields, using nanocrystals containing only a small number of molecules, or helical molecules, or icosahedral virus particles up to 10-20 times longer pulses can be tolerated, see Figure 4d.

## IMAGE RECONSTRUCTION

A number of methods exist for recovering phases for objects that have a finite size, or "support". These include oversampling of continuous molecular transforms [22 Bates, 1982; 23 Fienup, 1982; 24 Sayre, 1990; 25 Szöke 1999; 4 Miao et al., 1999], holographic imaging methods [26 Szöke, 1986; 27 Tegze and Faigel, 1991; 28 1996], holographic data evaluation methods [29 Szöke, 1993; 30 1997], classical methods of crystallography, and techniques for phase extension from lower resolution electron/X-ray cryo-microscopy images.

The past few years have seen the development of robust algorithms in solving the phase problem through oversampling the diffraction pattern, and this seems to be a most promising technique for the future. The 3D diffraction transform of a non-periodic particle is continuous. Only the diffraction amplitudes are sampled at discrete points by the pixellated detector and the process of classification. The measured diffraction intensities are proportional to the modulus squared of the Fourier transform of the wave exiting the object. On their own, these diffraction intensities are insufficient to back-transform to form an image in real space. That inversion requires knowledge of both the diffraction intensity and phase. If the diffraction pattern intensities are sampled finely enough, then it is possible to solve for the diffraction pattern phases [22 Bates, 1982; 23 Fienup, 1982]. The solution to this non-linear inversion problem is usually obtained iteratively by sequentially enforcing known constraints in reciprocal space and in real space. Specifically, in real space we assert that the image has zero scattering strength outside the area of the object's boundary (called its support) [23 Fienup, 1982], whilst in reciprocal space the squared modulus of the Fourier transform of the image must equal the measured diffraction intensities. Such algorithms have now been used successfully for image reconstruction in X-ray diffraction experiments [4 Miao, 1999; 31 Robinson, 2001; 32 He, 2003; 5 Marchesini, 2003b; 33 Williams, 2003; 34 Miao, 2003; 35 Shapiro, 2005; 6 Chapman, 2006]. An example of a reconstructed 3D image is shown in Figure 5.

The algorithms usually require that the support of the object be known *a priori*, and the closer the support to the actual object boundary, the better the reconstruction. The

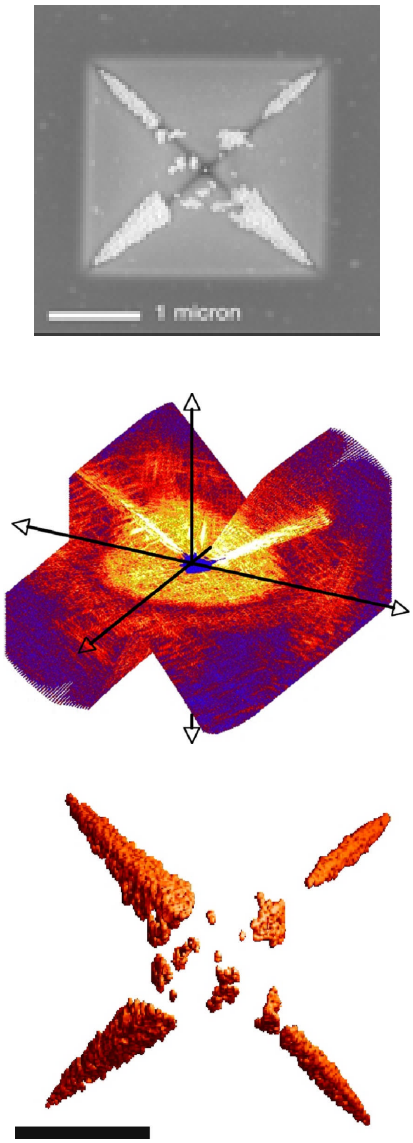


Figure 5: Coherent diffraction imaging and image reconstruction [6 Chapman et al., 2006]. Three-dimensional diffraction data (middle) recorded from a test object (top), consisting of 50-nm diameter gold balls on a silicon-nitride pyramid-shaped membrane, at a wavelength of 1.6 nm, and a rendering of the *ab initio* 3D image (bottom) reconstructed from the diffraction intensities to a resolution of 10 nm. The diffraction data were obtained by rotating the specimen in 1° increments from -70° to +70°, and then interpolated onto a $1024^3$-element array. A quadrant of the diffraction dataset has been removed for visualization in the central rendering of the 3D diffraction intensities. The gold balls seen in the rendering of the 3D reconstructed image on the right fill the inside edges of the silicon-nitride pyramid. The scale bar is 1 micron.

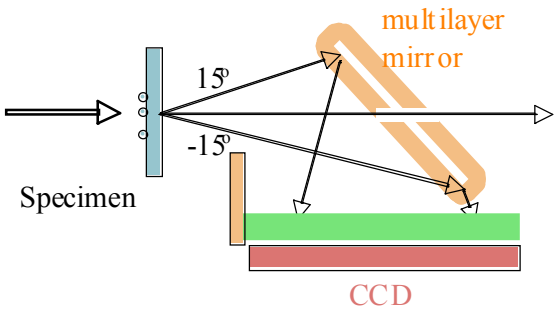


Figure 6: Schematic diagram of the diffraction camera for FLASH experiments, which uses a multilayer-coated mirror to reflect the diffraction pattern onto a CCD. The intense direct beam passes through a hole in the mirror.

algorithm called SHRINKWRAP successively refines an estimate of the support from a current estimate of the image [5 Marchesini, 2003]. This algorithm does not require the support to be known and is remarkably robust at finding the smallest image support that contains the majority of the image intensity.

## EXPERIMENTS AT FLASH

Experiments were carried out at FLASH (Free-electron LASer at Hamburg, formerly known as the VUV-FEL). During the experiments the machine operated at a wavelength of 32 nm and in the ultrafast pulse mode of 25 ± 5 fs duration [36 FEL]. The pulses were focused to a 20 μm spot on the sample by an ellipsoidal mirror, achieving intensities up to about $10^{14}$ W/cm$^2$. We carried out experiments to demonstrate ultrafast coherent diffraction imaging and to study the interaction of matter with FEL pulses, in order to constrain our models to determine ultimate resolution limits with XFELs.

Our experiments at FLASH depend critically on being able to measure the forward scattering from samples with high sensitivity and low noise or parasitic scattering. The main experimental challenge was to prevent the direct beam from hitting the direct-detection CCD and to prevent out of band radiation (plasma emission from the sample) or non-sample scatter from obscuring the coherent diffraction signals. We solved these problems using a flat mirror oriented at 45° to the beam. The direct beam passes through a hole in the mirror whereas the diffracted beam is reflected from the mirror onto a bare CCD. The camera records diffraction angles between –15° to +15°, which requires a multilayer coating on the mirror that varies in layer spacing by a factor of two over a distance of only 28 mm (Bajt et al, in preparation). The multilayer coating was challenging because of the low absorption length of materials at 32 nm wavelength. We designed a coating consisting of three layers (Si, Mo, and $B_4C$), which simultaneously met the requirements of low stress, high reflectivity at 32 nm, and high reflectivity at the characterization wavelength of 0.154 nm. An advantage of the multilayer mirror is that it acts as a bandpass filter both for wavelength and direction. Plasma emission from the sample in the UV and visible ranges is rejected by the mirror. Stray light, from the scattering of beamline optics for example, hit the mirror at an angle that does not obey the Bragg law, and hence was are also filtered out. Additionally, the mirror reflectivity diminishes smoothly to zero at the edge of the hole, due to roughness of the substrate at the edge. This "soft edge" reduces scatter from the hole.

We have performed several experiments using this apparatus, which will be reported on in forthcoming publications.

## REFERENCES

[1] Neutze, R. Wouts, D. van der Spoel, E. Weckert, and J. Hajdu, "Potential for biomolecular imaging with femtoscond X-ray pulses," Nature 406 (2000) 752.
[2] D. Sayre and H.N. Chapman, "X-ray microscopy," Acta Cryst. A. 51 (1995) 237.
[3] D. Sayre, "Some implications of a theorem due to Shannon," Acta Cryst. 5, (1952) 843.
[4] J. Miao, P. Charalambous, J. Kirz and D. Sayre, "Extending the methodology of x-ray crystallography to allow imaging of micrometre-sized non-crystalline specimens," Nature 400 (1999) 342.
[5] S. Marchesini *et al.* "X-ray image reconstruction from a diffraction pattern alone," Phys. Rev. B 68 (2003), 140101.
[6] H.N. Chapman *et al.* "High-resolution ab initio Three-dimensional X-ray Diffraction Microscopy," J. Opt. Soc. Am. A 23 (2006) 1179.
[7] J.C.H. Spence and R. B. Doak, "Single molecule diffraction," Phys. Rev. Lett. 92 (2004) 198102.
[8] D. Starodub *et al.* "Damped and thermal motion of laser-aligned hydrated macromolecule beams for diffraction," J. Chem. Phys 123 (2005) 24430.
[9] R. Henderson, "Cryoprotection of protein crystals against radiation-damage in electron and X-ray diffraction," Proc. R. Soc. 241 (1990) 6.
[10] R. Henderson, "The potential and limitations of neutrons, electrons and X-rays for atomic resolution microscopy of unstained biological molecules," Quart. Rev. Biophys. 28 (1995) 171.
[11] C. Nave, "Radiation damage in protein crystallography," Rad. Phys. Chem. 45 (1995) 483.
[12] M.R. Howells *et al.*, "An assessment of the resolution limitation due to radiation-damage in x-ray diffraction microscopy," http://arxiv.org/physics/0502059
[13] Z. Jurek, G. Faigel, and M. Tegze, "Dynamics in a cluster under the influence of intense femtosecond hard x-ray pulses," Euro. Phys. J. D 29 (2004) 217.
[14] Z. Jurek, G. Oszlanyi and G. Faigel, "Imaging atom-clusters by hard x-ray free electron lasers," Europhys Lett., 65 (2005) 491.

[15] S.P. Hau-Riege, R.A London and A. Szöke, "Dynamics of X-Ray Irradiated Biological Molecules," Phys. Rev. E 69 (2004) 051906.
[16] M.Bergh, N. Timneanu and D. van der Spoel, "A Model for the Dynamics of a Water Cluster in an X-ray Free Electron Laser Beam," Phys. Rev. E 70 (2004) 051904.
[17] R.A. London, A. Szoke, and S.P. Hau-Riege, "A tamper to delay the motion of a sample during irradiation by short intense x-ray pulses," patent pending (2006).
[18] J. Frank, "Three-Dimensional Electron Microscopy of Macromolecular Assemblies," Academic Press, San Diego (1996).
[19] M. van Heel *et al.* "Single-particle electron cryo-microscopy: towards atomic resolution," Quart. Rev. Biophys. 33 (2000) 307.
[20] G. Huldt, A. Szöke and J. Hajdu, "Diffraction imaging of single particles and biomolecules," J. Struct. Biol. 144 (2003) 219.
[21] S.P. Hau-Riege, R.A. London, G. Huldt and H.N. Chapman, "Pulse requirements for x-ray diffraction imaging of single biological molecules," Phys. Rev. E 71 (2005) 061919.
[22] R.H.T. Bates, "Fourier phase problems are uniquely solvable in more than one dimension. 1. Underlying theory," Optik 61 (1982) 247.
[23] J.R. Fienup, "Phase retrieval algorithms-a comparison," Appl. Opt. 21 (1982) 2758.
[24] D. Sayre in Proceedings of the 1990 NATO Course, Erice (H. Schenk, ed.) (1991) p.353.
[25] A. Szöke, "Time-resolved holographic diffraction at atomic resolution," Chem. Phys. Letts. 313 (1999) 777.
[26] A. Szöke, "X-ray and electron holography using a local reference beam," in Short Wavelength Coherent Radiation: Generation and Application. Attwood, D. T. and Bokor, J. eds., American Institute of Physics Conference Proceedings No. 147, New York (1986).
[27] M. Tegze and G. Faigel, "Atomic-resolution X-ray holography," Europhys. Lett. 16 (1991) 41.
[28] M. Tegze and G. Faigel, "X-ray holography with atomic resolution," Nature 380 (1996) 49.
[29] A. Szöke, "Holographic methods in X-ray crystallography. 2. Detailed theory and connection to other methods of crystallography," Act. Cryst. A 49 (1993) 853.
[30] A. Szöke, H. Szöke and J.R. Somoza, "Holographic methods in X-ray crystallography 5. Multiple isomorphous replacement, multiple anomalous dispersion and non- crystallographic symmetry," Acta Cryst. A 53 (1997) 291.
[31] I.K. Robinson, I.A. Vartanyants, G.J. Williams, M.A. Pfeifer and J.A. Pitney, "Reconstruction of the shapes of gold nanocrystals using coherent x-ray diffraction," Phys. Rev. Lett., 87 (2001) 195505.
[32] H. He, S. Marchesini, M. Howells, U. Weierstall, G. Hembree, and J. C. H. Spence, "Experimental lensless soft-x-ray imaging using iterative algorithms: phasing diffuse scattering," Acta Cryst. A 59 (2003) 143.
[33] G. J. Williams, M. A. Pfeifer, I. A. Vartanyants, and I. K. Robinson, "Three-dimensional imaging of microstructure in Au nanocrystals," Phys. Rev. Lett. 90 (2003) 175501.
[34] J. Miao, T. Ishikawa, E. H. Anderson, and K. O. Hodgson, "Phase retrieval of diffraction patterns from noncrystalline samples using the oversampling method," Phys. Rev. B 67 (2003) 174104.
[35] D. Shapiro, P. Thibault, T. Beetz, V. Elser, M. Howells, C. Jacobsen, J. Kirz, E. Lima, H. Miao, A. M. Neimann, and D. Sayre, "Biological imaging by soft x-ray diffraction microscopy," Proc. Natl. Acad. Sci. U.S.A. 102 (2005) 15343.
[36] V. Ayvazyan *et al.,* "First operation of a free-electron laser generating GW power radiation at 32 nm wavelength," Eur. Phys. J. D 37 (2006) 297.